LAGRANGIAN EVOLUTION OF HAIRPIN STRUCTURES IN THE TEMPORAL TRANSITION IN CHANNEL FLOW

Yaomin Zhao
State Key Laboratory for Turbulence and Complex Systems
College of Engineering, Peking University
Beijing 100871, China
zym89@pku.edu.cn

Yue Yang
State Key Laboratory for Turbulence and Complex Systems
College of Engineering, Peking University
Beijing 100871, China
yyg@pku.edu.cn

Shiyi Chen
State Key Laboratory for Turbulence and Complex Systems
College of Engineering, Peking University
Beijing 100871, China
syc@pku.edu.cn

ABSTRACT

A Lagrangian study on the evolution of vortical structures in the Klebanoff-type temporal transitional channel flow is reported. Based on the Eulerian velocity field from the direct numerical simulation, a backward-particle-tracking method is applied to solve the transport equation of the Lagrangian scalar field. and then the iso-surfaces of the Lagrangian field can be extracted as Lagrangian material surfaces in the evolution. It is noted that the Lagrangian surface, which is initially a vortex surface, is demonstrated as a good approximation of a vortex surface before significant topological changes. Thus the Lagrangian structures can be used to represent the evolution of vortical structures in the early transition. The evolution of a typical Lagrangian surface is presented. The near-wall Lagrangian surface can evolve from a streamwise-spanwise sheet to a triangular bulge, and then into the signature hairpin-like structure. By comparing the Lagrangian results with the vortical structures identified by Eulerian vortex identification criteria, differences between Lagrangian and Eulerian structures are discussed. In particular, the Lagrangian approach can elucidate the continuous temporal evolution of vortical structures in transitional wall flows.

INTRODUCTION

The laminar-turbulent transition has been one of the most fundamental and challenging problems in turbulence research for decades. The K-type transition is often used as a typical case to study transitional flows. Previous studies about the K-type transition provide an overview of the developing process of the transitional flow, and the formation and evolution of vortical structures play an important role (see Lee & Wu, 2008).

In the vortical structures, the 'hairpin vortex', first proposed by Theodorsen (1952), is considered as the key structure in turbulent wall flows that is closely related to the bursting process in the buffer layer. This kind of structures were visualized by smoke in the experiment by Head & Bandyopadhyay (1981), which demonstrates that turbulent boundary layer appears to consist very largely of hairpin vortices and related structures. Based on the concept of the hairpin vortex and the attached-eddy hypothesis of Townsend (1976), Perry & Chong (1982) proposed a model for wall turbulence, connecting the turbulent statistics with the randomly scattered hairpin vortices. This model was then extended in the work of Perry *et al.* (1986) and Perry & Marusic (1995).

Although some models of wall turbulence based on the concept of hairpin vortices or quasi-streamwise vortices have been developed, our understanding of hairpin vortices are still not complete. Robinson (1991) claimed that hairpins with a pair of counter-rotating quasi-steamwise vortices play some role in the dynamics of wall-bounded turbulent flows, but the details are still controversial. The recent development of numerical simulation and high-resolution particle image velocimetry (PIV) technique provides more information about hairpin vortices and related structures in wall turbulence. Zhou *et al.* (1999) discussed the mechanism of the evolution of a single hairpin vortex-like structure into coherent packets of hairpin vortices in a low-Reynolds-number channel flow. Combining PIV experiments and direct numerical simulations, Adrian (2007) thoroughly reviewed the dynamics of hairpin vortex and hairpin packets,

1

and pointed out that turbulent statistics such as turbulent kinetic energy and Reynolds stress are highly correlated with hairpin-related structures. Based on the increasing understanding of coherent structures in wall-bounded turbulence, Marusic *et al.* (2010) proposed a wall model which can predict near-wall velocity profile relying on large-scale motions in the outer layer. These studies about hairpin vortices, however, are mainly based on the vortical structures identified from Eulerian velocity fields at a time instant, so there is still a lack of a description for the dynamic, continuous temporal evolution of vortical structures.

For studying the vortical structures in wall turbulence, the vortex identification methods are of importantce, and they can be roughly divided into two categories. One is based on Eulerian criteria, and the other is from the Lagrangian perspective. Since the Eulerian identification methods are based on instantaneous velocity fields, in principle, the information of dynamic evolution of the vortex structures at different times is missing. On the other hand, the Lagrangian vortex identification methods appear to be more natural to describe the evolution of vortical structures than the Eulerian methods. In experiments, visualization techniques such as smoke, dye and hydrogen bubbles are typical Lagrangian-type methods. However, these methods face difficulties of diffusion or following property of the tracers, and they can hardly be used for quantitative analysis (see Robinson, 1991). In numerical simulations, a few of Lagrangian-type vortex identification methods were proposed. Haller (2001) used the direct Lyapunov exponent to define 'Lagrangian coherent structures' in three-dimensional flow. This method was applied to study the evolution of a single hairpin vortex and coherent structures in fully developed wall turbulence (Green *et al.*, 2007).

Based on tracking of Lagrangian material surface, the Lagrangian scalar field and related multi-scale geometric analysis have been successfully applied in isotropic turbulence (Yang *et al.*, 2010), simple transitional flows such as Taylor-Green and Kida-Pelz flows (Yang & Pullin, 2010), and fully developed channel flows (Yang & Pullin, 2011b). This method can present the temporal evolution of Lagrangian surfaces with quantitative multi-scale and multi-directional statistical geometry. In the present study, this method is extended to the laminar-turbulent transition problem. By investigating the dynamic evolution of Lagrangian structures in transitional channel flow, we provide a Lagrangian perspective to elucidate the dynamics in the formation and evolution of the typical vortical structures.

METHODS
Direct numerical simulation of temporal transitional channel flow

A diagram of the computation domain of channel flow is shown in figure 1. The sides of the domain in the streamwise x-, the spanwise y- and the wall-normal z- directions are L_x, L_y and L_z, respectively. The three-dimensional incompressible Navier-Stokes equations for the velocity $\boldsymbol{u} = (u, v, w)$ are non-dimensionalized by the channel half-height δ and the bulk velocity U_b as

$$\left.\begin{array}{l} \dfrac{\partial \boldsymbol{u}}{\partial t} + \boldsymbol{u} \cdot \boldsymbol{\nabla} \boldsymbol{u} = -\nabla p + \boldsymbol{f} + \dfrac{1}{Re_b} \nabla^2 \boldsymbol{u}, \\[2mm] \boldsymbol{\nabla} \cdot \boldsymbol{u} = 0, \end{array}\right\} \qquad (1)$$
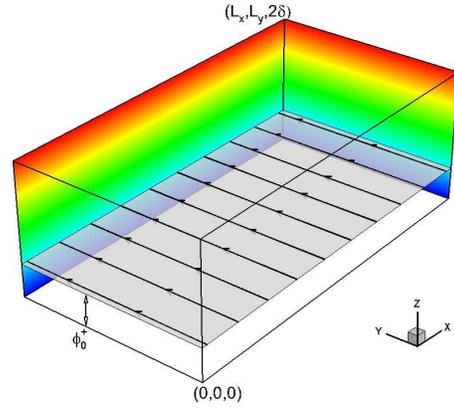
Figure 1.   Diagram of the computational domain.

where p is the pressure, ν is the kinetic viscosity, $Re_b = U_b \delta / \nu$ denotes the Reynolds number with $U_b = \int_0^{2\delta} u \, dz / L_z$. The channel half-height is set as $\delta = 1$, and the flow is driven by a time-dependent external force $\boldsymbol{f}(t)$ to maintain a constant flow flux with $U_b \approx 1$ in the streamwise direction.

For the direct numerical simulation (DNS), (1) is solved by the Fourier–Chebyshev pseudo-spectral method (Kim *et al.*, 1987). The no-slip conditions are applied at the walls at $z = 0$ and $z = 2\delta$, and the periodic boundary conditions are applied in the streamwise and spanwise directions. The nonlinear term is dealiased using the two-thirds truncation method (Canuto *et al.*, 1988). The low-storage third-order semi-implicit Runge-Kutta method (Spalart *et al.*, 1991) is applied for the temporal discretization. The number of grids N_x, N_y and N_z in all the directions and other parameters of the simulations are listed in table 1. The wall-friction Reynolds number $Re_\tau = u_\tau \delta / \nu$ in this table is calculated after the flow reaches the fully developed turbulent state, where $u_\tau = \sqrt{\tau_w / \rho}$ is the wall friction velocity with wall shear stress τ_w.

Table 1.   Summary of DNS parameters.

Re_τ	L_x	L_y	L_z	N_x	N_y	N_z
207.8	5.61	2.99	2	192	192	192

The initial condition is set as the basic Poiseuille flow with three Tollmien–Schlichting (TS) waves to trigger the K-type transition. The initial disturbances (see Sandham & Kleiser, 1992; Schlatter *et al.*, 2004) consist of a two-dimensional TS wave with an amplitude of $A_1 = 3.5\%$ and a pair of superimposed oblique three-dimensional waves with amplitudes of $A_2 = 0.09\%$, which are similar to the simulations in Gilbert & Kleiser (1990). The numerical solver and initial disturbances used in this DNS were verified in Zhao *et al.* (2014).

The flow gradually evolves from the laminar state into the fully developed turbulent state with the imposed initial disturbances. The temporal evolution of the wall-friction Reynolds number Re_τ is shown in figure 2. The transition in this simulation can be roughly divided into three

2
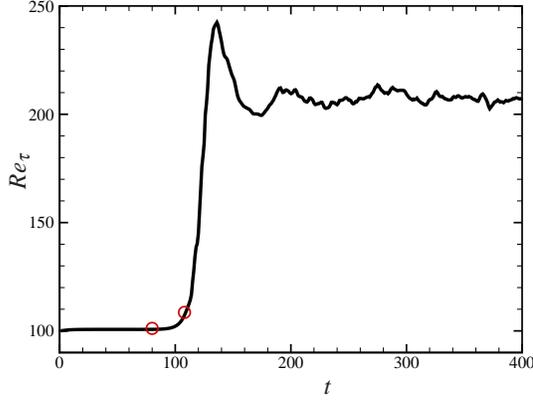
Figure 2. Temporal evolution of the wall-Reynolds number Re_τ in the K-type temporal transition in a channel flow. The initial and ending tracking times are marked by red circles.

Figure 3. Temporal evolution of $\langle \lambda_\omega \rangle$, where λ_ω is the cosine of the angle between $\boldsymbol{\omega}$ and $\boldsymbol{\nabla}\phi$. The dashed line shows the 5% level.

stages. First, the initial disturbances gradually amplify at $t < 80$, with the integral flow quantities such as Re_τ remain at the laminar values. After the slow amplification of the disturbances, the integral quantities change significantly in a short period, which implies the onset of the transition at $80 \leq t \leq 108$. The flow structures undergo significant topological changes around $t = 108$, and then the flow develops into the fully turbulent state. The evolution of flow structures in the early transitional stage for $80 \leq t \leq 108$ will be studied in detail.

Backward-particle-tracking method for the Lagrangian field

The equation for the Lagrangian scalar field $\phi(\boldsymbol{x}, t)$ in incompressible flow reads

$$\frac{\partial \phi}{\partial t} + \boldsymbol{u} \cdot \boldsymbol{\nabla}\phi = 0, \qquad (2)$$

and iso-surfaces of the scalar field are Lagrangian material surfaces in the temporal evolution. A set of ordinary differential equations (ODEs) are converted from (2) to calculate trajectories of fluid particles as

$$\frac{\partial \boldsymbol{X}(\boldsymbol{x}_0, t_0 \mid t)}{\partial t} = \boldsymbol{V}(\boldsymbol{x}_0, t_0 \mid t) = \boldsymbol{u}(\boldsymbol{X}(\boldsymbol{x}_0, t_0 \mid t), t), \qquad (3)$$

where $\boldsymbol{X}(\boldsymbol{x}_0, t_0 \mid t)$ is the location at time t of the particle which was located at $\boldsymbol{x}_0$ at the initial time t_0 and $\boldsymbol{V}(\boldsymbol{x}_0, t_0 \mid t)$ is the particle velocity at time t. A backward-particle-tracking method is implemented to solve (3). More details about this numerical scheme should be referred to Yang et al. (2010) and Yang & Pullin (2011b).

The initial Lagrangian field is set as $\phi_0 = z$, and the iso-surfaces of $\phi(\boldsymbol{x}_0, t_0)$ are streamwise-spanwise planes at different wall distances in figure 1. It is noted that the Lagrangian field stays invariant for this particular ϕ_0 in the perfect laminar Poiseuille flow, while imposed initial disturbances, can break the invariance and cause the evolution

of the scalar field. The initial tracing time $t_0 = 80$ is selected when the amplitudes of the initial disturbances are small enough, so that every initial material surface can be approximated as a vortex sheet that is composed of vortex lines.

The evolution and dynamics of Lagrangian structures can be studied from the evolution of Lagrangian material surfaces in the early transitional stage for $80 \leq t \leq 108$. The Lagrangian surface extracted as the iso-surface of the Lagrangian field with contour level $\phi_0^+ = 45$ are selected to study the evolution of Lagrangian hairpin structures. Here, $\phi_0^+ = \phi_0/\delta_v$ is the scaled initial scalar value at $t = t_0$. Hence, the surface of $\phi_0^+ = 45$ is from the log-law region. With the initial field $\phi_0 = z$, the scalar value on the surface remains a constant from the mapping

$$\phi^+(\boldsymbol{x}, t) = \phi^+(\boldsymbol{X}(\boldsymbol{x}_0, t_0 \mid t), t) \longleftrightarrow \phi^+(\boldsymbol{x}_0, t_0) \longleftrightarrow z_0^+. \quad (4)$$

Approximation of vortex surfaces

As remarked in Yang & Pullin (2010), the Lagrangian surface can be considered as a good approximation for the vortex surface before significant topological changes in high-Reynolds-number flows. The vortex surface is a surface composed of vortex lines, which implies that the local vorticity vector is tangent at every point on the surface. Since the flow at the initial time t_0 is a laminar Poiseuille flow with small disturbances, and the vorticity then mainly has the spanwise y-component, the initial Lagrangian surface $\phi_0 = z_0$ can be taken as a good approximation of the vortex surface, which is sketched in figure 1.

The cosine λ_ω of the angle between the vorticity and the Lagrangian scalar gradient can be used to quantify the approximation of a Lagrangian surface to a vortex surface (see Yang et al., 2010; Yang & Pullin, 2011a). Here, λ_ω is defined as

$$\lambda_\omega \equiv \frac{\boldsymbol{\omega} \cdot \boldsymbol{n}}{|\boldsymbol{\omega}|}. \qquad (5)$$

If $\boldsymbol{\omega}$ is perpendicular to $\boldsymbol{n}$ in the whole field, the Lagrangian surfaces completely coincide with the vortex surfaces with $\langle \lambda_\omega \rangle = 0$, where $\langle \cdot \rangle$ denotes the volume average.

3

Temporal evolution of $\langle \lambda_\omega \rangle$ obtained from the present transitional channel flow is shown in figure 3. For strictly inviscid incompressible flow with conservative body forces, the Helmholtz vorticity theorem shows that Lagrangian surfaces which are vortex surfaces at time $t = 0$ remain so for $t > 0$. Thus $\langle \lambda_\omega \rangle = 0$ can be satisfied for $t > 0$ with $\langle \lambda_\omega \rangle = 0$ at $t = 0$ in inviscid flow. In a viscous flow, as shown in figure 3, $\langle \lambda_\omega \rangle$ slowly increases because of the viscous effect and the breakdown of the Helmholtz theorem. However, $\langle \lambda_\omega \rangle$ remains less than the 10% level for $t < 108$ in the present transitional flow. Therefore, we can reasonably assume that vortex surfaces are still well approximated by the Lagrangian surfaces at the early stage of transition before significant topological changes of vortical structures. In order to ensure the good approximation of vortex surfaces using Lagrangian surfaces, the results in the present study are restricted on the evolution for $80 \leq t \leq 108$ with $\langle \lambda_\omega \rangle \leq 10\%$.

RESULTS: ANALYSIS OF LAGRANGIAN HAIRPIN STRUCTURES

In this section, the evolution and dynamics of the Lagrangian hairpin-like structures is investigated using the Lagrangian surface $\phi_0^+ = 45$, which can evolve from a streamwise-spanwise sheet to a triangular bulge, and then into the signature hairpin-like structure. The iso-surfaces of the Eulerian vortex identification criteria is also used for comparison.

Stage 1, triangular bulge

The so-called 'Λ-vortex' is frequently mentioned in the transition research, and it is often considered as a prior stage of hairpin vortices (Sandham & Kleiser, 1992). The 'Λ-vortex' identified by the λ_2-criterion in the present transitional channel flow is shown in figure 4(b). At the mean time, vortex lines, colour-coded by the magnitude of vorticity, are integrated and drawn near the λ_2 iso-surface, but tube-like vortical structures cannot be identified from the vortex lines.

For comparison, the Lagrangian surface presented in figure 4(a) at the same time $t = 100$ shows a triangular bulge. We can see that the vortex lines drawn in figure 4(a) are almost on the Lagrangian surface, which also demonstrates that the Lagrangian surface can be considered as a good approximation of the vortex surface. It is interesting to observe that the ridge of the Lagrangian triangular bulge coincides with the Eulerian 'Λ-vortex'. We can see that the vortex lines bend at the edge of the bulge, and vorticity components ω_x and ω_z have finite values in this region. From the Lagrangian study, the finite streamwise and wall-normal vorticities at the edge of the Lagrangian bulge are the essence of the 'Λ-vortex'.

Furthermore, from $|\boldsymbol{\omega}|$ on the vortex lines drawn in figure 4, there is no obvious vorticity intensification region near the triangular bulge. This indicates that the mean shear, rather than the vortical structures with obvious swirling motions, is dominating in the evolution of Lagrangian surfaces at this stage.

Stage 2, vorticity intensification

In this stage, the vorticity begins to be intensified in local regions and the tube-like vortical structures form as shown in figures 4 and 5. In this process, the evolution of vorticity becomes important, and the vortical structures start to play a key role in the evolution along with the background shear flow.

As shown in figure 4(a), the geometry of Lagrangian structures implies that the vortex lines attached on the surface bend near the ridge. This means that ω_z and ω_x are of finite amplitudes in this region from the inclination of vortex lines. Under the effect of the main flow shear, the voticity componets ω_x and ω_z increase in this region. This implies that the vortex lines are intensively stretched and the most intensified $|\boldsymbol{\omega}|$ occurs at the edge of the triangular bulge.

Furthermore, this process is led by the tip of the bulge where is the most distant from the wall in the Lagrangian structure. Moreover, the vortex lines at the tip are the most highly curved part, so they endure the largest mean shear and induced velocities. In the Lagrangian view, the bulge of the surface lifts and elongates in figure 4(a). Then the surface rolls up, and tube-like structures form at the tip in figure 5(a). The vortex lines are stretched in the streamwise direction because of the mean flow shear, and then they are folded inward at the neck. The folding vortex lines concentrate and they are rapidly stretched out with intensified $|\boldsymbol{\omega}|$. The arch (or head) of the hairpin-like structure are pulled out at this part of the Lagrangian structure.

Stage 3, hairpin-like structures

The 'hairpin vortex' is often described as the hairpin-shaped, tube-like structure. It is noted that the major structure of the hairpin can be captured by the Eulerian λ_2-criterion in figure 6(b), because the Eulerian criteria have the capability to identify the 'vortex core' at a time instant. However, the dynamic evolution of the hairpin-like structures cannot be observed from the Eulerian method in figures 4(b), 5(b) and 6(b). On the other hand, the dynamic mechanism of the Lagrangian hairpin structures is provided by the typical Lagrangian surface presented in figures 4(a), 5(a) and 6(a). In the evolution, the Lagrangian hairpin-like structure are streached out from the triangular bulge at $t = 106$ in figure 6(a) after the vorticity intensification stage. At the stage after $t = 106$, the vorticity distribution of the hairpin structures could be considered as isolated, thin and elongated vortex tubes or filaments.

The vortex-induced velocity at this stage can be calculated by the Biot-Savart law. The geometry of vortex lines is important in dynamics because the motion of vortex lines and the Lagrangian surfaces is affected by the self-induced velocity of the hairpin structures. The induced-velocity at the tip of the hairpin-like structure is upper backward, so the hairpin lifts under its self-induction. On the other hand, the hairpin-like structure elongates in the streamwise direction controlled by the background shear flow. Under both effects, the primary hairpin is lifted and stretched.

CONCLUSION

The Lagrangian scalar field is applied in the K-type transitional channel flow. By tracking the Lagrangian field, we are able to investigate the evolution of the Lagrangian structures as the iso-surfaces of the Lagrangian field. The most typical Lagrangian surface, initially located in the logarithm layer, evolves from the streamwise-spanwise plane to the triangular bulge, and then into the signature hairpin-like structures. In the evolution, the Lagrangian surfaces can be approximated as vortex surfaces before significant

(a)   (b)
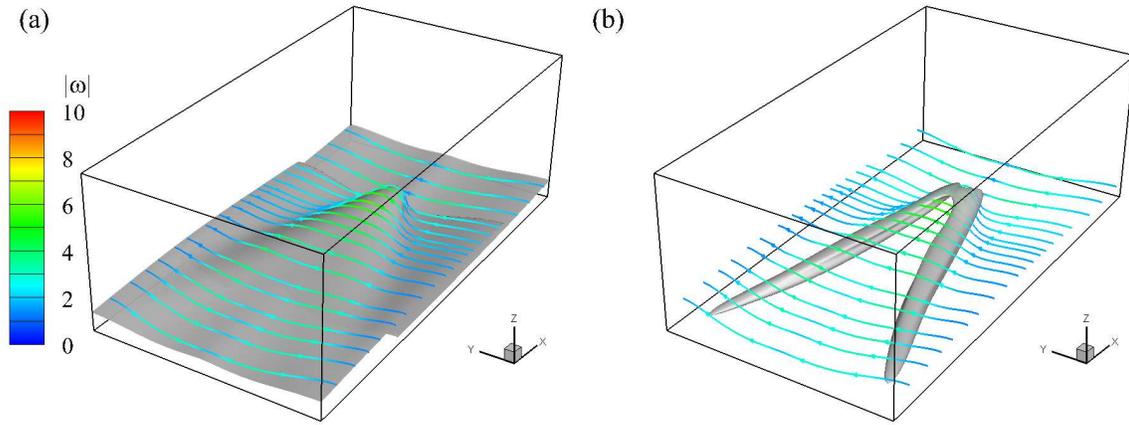
Figure 4.   Comparison of Lagrangian and Eulerian vortical structures at $t = 100$. Vortex lines are integrated and drawn on the surfaces, and colour-coded by the magnitude of vorticity $|\boldsymbol{\omega}|$. (a) Lagrangian surface of $\phi_0^+ = 45$, (b) iso-surface of λ_2.

(a)   (b)
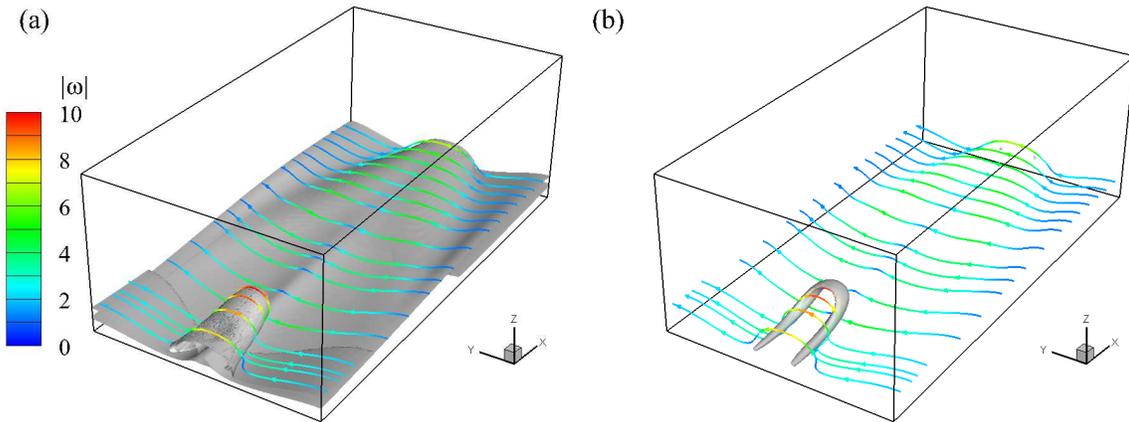
Figure 5.   Comparison of Lagrangian and Eulerian vortex structures at $t = 104$. Vortex lines are integrated and drawn on the surfaces, and colour-coded by the magnitude of vorticity $|\boldsymbol{\omega}|$. (a) Lagrangian surface of $\phi_0^+ = 45$, (b) iso-surface of λ_2.

(a)   (b)
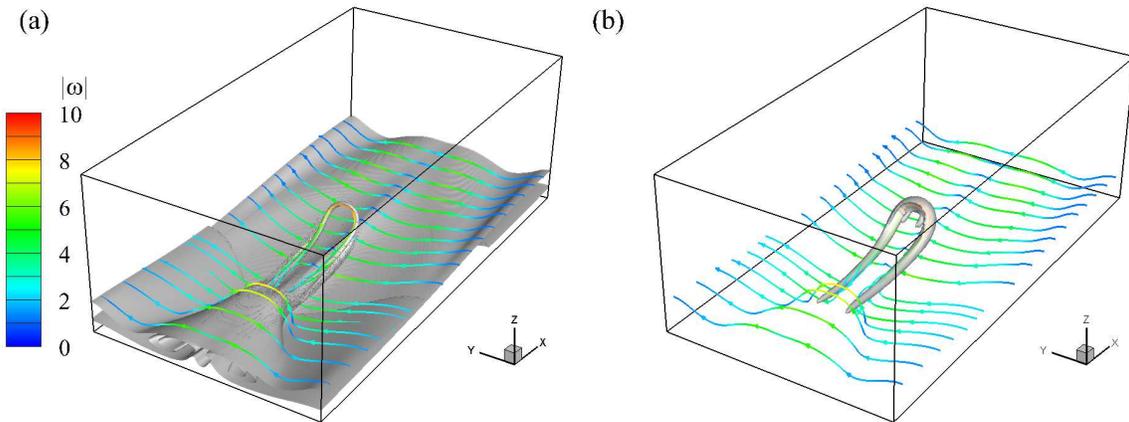
Figure 6.   Comparison of Lagrangian and Eulerian vortex structures at $t = 106$. Vortex lines are integrated and drawn on the surfaces, and colour-coded by the magnitude of vorticity $|\boldsymbol{\omega}|$. (a) Lagrangian surface of $\phi_0^+ = 45$, (b) iso-surface of λ_2.

topological changes. Therefore, the present study provides a dynamic view of the evolving vortical structures in temporal transitional flow in a Lagrangian perspective.

As the flow evolves, the amplitudes of the disturbances are intensified. Then the vortical structure gradually forms and begins to play an important role. The intensification of the vorticity mainly exhibits at the edge of the triangular bulge. With the concentrating vortex lines, the Lagrangian surface rolls up into the hairpin-shaped, tube-like structure. The evolution of the Lagrangian hairpin-like structure can be approximated as a vortex filament and described by the Biot-Savart law. Under the effect of the mean shear and the self-induction, the hairpin-like structure lifts and elongates.

In summary, the formation and evolution of the Lagrangian structures are extensively studied in a Lagrangian perspective. Some similarities and differences with the results from the Eulerian vortex identification criteria are discussed. It is noted that the continuous temporal evolution of vortical structures can be elucidated by tracking a unique Lagrangian surface, which is unlikely using Eulerian methods.

We remark that the present work only focus on the early transitional stage, because the deviation between the Lagrangian surfaces and the vortex surfaces cannot be ignored after the significant topological changes or vortex reconnections. Thus, a vortex-surface-field method (Yang & Pullin, 2011a; Pullin & Yang, 2014) should be applied to study the flow in the late transition in future work. Moreover, the current methodology can be easily applied to other transitional flows with a sequence of well resolved three-dimensional velocity data sets from numerical simulations or experiments.

REFERENCES

Adrian, R. J. 2007 Hairpin vortex organization in wall turbulence. *Phys. Fluids* **19**, 41301.

Canuto, C., Hussaini, M. Y., Quateroni, A. & Zang, T. A. 1988 *Spectral Methods in Fluid Dynamics*. Springer.

Gilbert, N. & Kleiser, L. 1990 Near-wall phenomena in transition to turbulence. In *Near Wall Turbulence* (ed. S. J. Kline & N. H. Afgan), pp. 7–27. Hemisphere.

Green, M. A., Rowley, C. W. & Haller, G. 2007 Detection of Lagrangian coherent structures in three-dimensional turbulence. *J. Fluid Mech.* **572**, 111–120.

Haller, G. 2001 Distinguished material surfaces and coherent structures in three-dimensional fluid flows. *Physica D* **149**, 248–277.

Head, M. R. & Bandyopadhyay, P. 1981 New aspects of turbulent boundary-layer structure. *J. Fluid Mech.* **107**, 297–338.

Kim, J., Moin, P. & Moser, R. D. 1987 Turbulent statistics in fully developed channel flow at low Reynolds number. *J. Fluid Mech* **177**, 133–166.

Lee, C. B. & Wu, J. Z. 2008 Transition in wall-bounded flows. *Appl. Mech. Rev.* **61**, 030802.

Marusic, I., Mathis, R. & Hutchins, N. 2010 Predictive model for wall-bounded turbulent flow. *Science* **329**, 193–196.

Perry, A. E. & Chong, M. S. 1982 On the mechanism of wall turbulence. *J. Fluid Mech.* **119**, 173–217.

Perry, A. E., Henbest, S. & Chong, M. S. 1986 A theoretical and experimental study of wall turbulence. *J. Fluid Mech.* **165**, 163–199.

Perry, A. E. & Marusic, I. 1995 A wall-wake model for the turbulence structure of boundary-layers. Part 1. extension of the attached eddy hypothesis. *J. Fluid Mech.* **298**, 361–388.

Pullin, D. I. & Yang, Y. 2014 Whither vortex tubes? *Fluid Dyn. Res.* **46**, 0141618.

Robinson, S. K. 1991 Coherent motions in the turbulent boundary layer. *Annu. Rev. Fluid Mech.* **23**, 601–639.

Sandham, N. D. & Kleiser, L. 1992 The late stages of transition to turbulence in channel flow. *J. Fluid Mech.* **245**, 319–348.

Schlatter, P., Stolz, S. & Kleiser, L. 2004 LES of transitional flow using the approximate deconvolution model. *Int. J. Heat Fluid Flow* **25** (3), 549–558.

Spalart, P. R., Moser, R. D. & Rogers, M. M. 1991 Spectral methods for the Navier-Stokes equations with one infinite and two periodic directions. *J. Comput. Phys.* **96**, 297–324.

Theodorsen, T. 1952 Mechanism of turbulence. In *Proceedings of the Second Midwestern Conference on Fluid Mechanics*, pp. 1–18. Columbus.

Townsend, A. A. 1976 *The Structure of Turbulent Shear Flow*. Cambridge University Press.

Yang, Y. & Pullin, D. I. 2010 On Lagrangian and vortex-surface fields for flows with Taylor-Green and Kida-Pelz initial conditions. *J. Fluid Mech.* **661**, 446–481.

Yang, Y. & Pullin, D. I. 2011a Evolution of vortex-surface fields in viscous Taylor-Green and Kida-Pelz flows. *J. Fluid Mech.* **685**, 146–164.

Yang, Y. & Pullin, D. I. 2011b Geometric study of Lagrangian and Eulerian structures in turbulent channel flow. *J. Fluid Mech.* **674**, 67–92.

Yang, Y., Pullin, D. I. & Bermejo-Moreno, I. 2010 Multiscale geometric analysis of Lagrangian structures in isotropic turbulence. *J. Fluid Mech.* **654**, 233–270.

Zhao, Y., Xia, Z., Shi, Y., Xiao, Z. & Chen, S. 2014 Constrained large-eddy simulation of laminar-turbulent transition in channel flow. *Phys. Fluids* **26**, 095103.

Zhou, J., Adrian, R. J., Balachandar, S. & Kendall, T. M. 1999 Mechanisms for generating coherent packets of hairpin vortices in channel flow. *J. Fluid Mech.* **387**, 353–396.